



**CRITICAL RAW MATERIAL ELECTROCATALYSTS REPLACEMENT
ENABLING DESIGNED POST-2020 PEMFC**

Grant agreement no.: 779366

Start date: 01.01.2018 – Duration: 36 months

Project Coordinator: Deborah Jones – CNRS

DELIVERABLE REPORT

DELIVERABLE D3.1– SITE DENSITY AND TURN OVER FREQUENCY OF SELECTED BENCHMARK CATALYSTS

Due Date	30th April 2018
Author (s)	Mathias Primbs, Peter Strasser, Deborah Jones, Frederic Jaouen, Aaron Roy, Pierre-Yves Blanchard, Moulay Tahar Sougrati, Daniel Malko, Anthony Kucernak, Gaetano Granozzi, Christian Durante, Tomasz Kosmala, Valentina Perazzolo, Jonathan Sharman
Workpackage	WP3
Workpackage Leader	TUB
Lead Beneficiary	TUB
Date released by WP leader	8th May 2018
Date released by Coordinator	9th May 2018

DISSEMINATION LEVEL

PU	<i>Public</i>	x
PP	<i>Restricted to other programme participants (including the Commission Services)</i>	
RE	<i>Restricted to a group specified by the consortium (including the Commission Services)</i>	
CO	<i>Confidential, only for members of the consortium (including the Commission Services)</i>	

NATURE OF THE DELIVERABLE		
R	<i>Report</i>	x
P	<i>Prototype</i>	
D	<i>Demonstrator</i>	
O	<i>Other</i>	

SUMMARY	
Keywords	<i>Benchmark, SD, TOF</i>
Abstract	<i>This deliverable report describes the benchmarking of four non-platinum group metal (non-PGM) containing catalysts, consisting of key performance metrics, such as electrocatalytic mass activity (MA), selectivity, site density (SD) and catalytic turnover frequency (TOF). SD and TOF were evaluated using in situ nitrate reduction and ex situ low temperature CO chemisorption in combination with rotating ring disk electrode (RRDE) measurements. The iron coordination environment was determined by ⁵⁷Fe Mössbauer spectroscopy. Surface area and pore volume were determined from nitrogen adsorption isotherms. Electrochemical measurements were performed with a RRDE to determine the kinetic current and the selectivity of the catalysts to the oxygen reduction reaction (ORR). The properties of these benchmark catalysts will be used as a baseline to guide needs to increase the SD or TOF to reach the activity targets of the project, and to better assess the activity improvements realised with the new non-PGM catalysts prepared in CRESCENDO.</i>
Public abstract <i>(if different from the above)</i>	

REVISIONS			
Version	Date	Changed by	Comments
0.1			

SITE DENSITY AND TURN OVER FREQUENCY OF SELECTED BENCHMARK CATALYSTS

CONTENTS

1. Introduction.....	4
2. Experimental	4
2.1 Electrochemical Measurements	5
2.2 Nitrogen Physisorption	6
2.3 X-ray Photoelectron Spectroscopy	7
2.4 ⁵⁷ Fe Mössbauer Spectroscopy	7
2.5 Dynamic Light Scattering (DLS).....	7
2.6 CO-Chemisorption	8
2.7 Nitrite Reduction	10
3. Results and Discussion	11
3.1 Electrochemical Measurements – SD and TOF.....	11
3.2 Physicochemical Characterisation	17
4. Conclusions and Future Work	26
5. Reference	26

1. INTRODUCTION

This deliverable report describes the benchmarking, consisting of key performance metrics, including electrocatalytic mass activity (MA), selectivity, site density (SD) and catalytic turnover frequency (TOF), of four non-platinum group (non-PGM) metal containing catalysts. SD and TOF were evaluated using in situ nitrate reduction and ex situ low temperature CO chemisorption in combination with rotating ring disk electrode (RRDE) measurements. The bulk and surface iron coordination environment was determined by ^{57}Fe Mössbauer spectroscopy and X-ray photoelectron spectroscopy respectively. Surface area and pore volume were derived from nitrogen adsorption isotherms. The kinetic current and the selectivity towards the oxygen reduction reaction (ORR) were determined from RRDE measurements before and after an accelerated stress test. The results will be used as a baseline to guide needs to increase either the SD or TOF to reach the activity targets of the project, and to better assess the activity improvements given by the new non-PGM catalysts prepared in work package 3.

The chosen materials are currently best-in-class non-PGM catalysts for PEMFC applications, including a Fe-doped ZIF-based catalyst, a polymer-derived catalyst and a commercial catalyst.

We assessed how the *ex situ* and *in situ* methodologies correlate with each other for SD determination, and with the measured ORR performance. This will establish a common base level activity to compare the newly developed catalysts.

2. EXPERIMENTAL

The study used a range of different experimental methods, performed by different partners as seen in **Table 1**.

Table 1: Experimental methods used by project partners

Method	Partners
Electrochemistry RRDE	CNRS, ICL, TUB, UNIPD
Nitrogen physisorption	UNIPD, ICL
X-ray photoelectron spectroscopy	UNIPD
^{57}Fe Mössbauer spectroscopy	CNRS, UNIPD
CO chemisorption	TUB
Nitrite reduction	ICL

The catalysts belong to the current best-in-class catalyst, denoted here as Catalyst 1, Catalyst 2, Catalyst 3 and Catalyst 4.

2.1 ELECTROCHEMICAL MEASUREMENTS

The electrochemical benchmark test consists of the determination of the catalytic activity via a rotating ring disk electrode set-up at two different catalyst loadings on the electrode, as well as an accelerated stress test (AST). The loadings of 0.8 mg cm^{-2} and 0.2 mg cm^{-2} were chosen to study the influence of layer thickness on the catalyst performance. The AST was performed with the electrode of lower loading.

Catalyst powder morphology

No milling of pyrolysed catalyst powder was applied systematically. However, the average particle size was measured with dynamic light scattering (DLS). If DLS showed that the average particle size is $> 1 \text{ }\mu\text{m}$, then planetary ball milling with zirconia vial and balls (400 rpm, 40 min, 5 mm zirconia balls, 50/50 IPA/water slurry) was applied and DLS performed again, with the aim of reaching an average particle size below $1 \text{ }\mu\text{m}$, more appropriate to prepare catalyst inks and to promote smooth and uniform RDE layers.

Ink formulation

The catalyst ink consisted of a slurry of the catalyst, isopropanol and ultrapure water in a mass ratio of 1:1 and Nafion (5 wt%, Sigma-Aldrich). The catalyst content was 0.5 wt% (0.2 mg cm^{-2} loading) and 2.0 wt% (0.8 mg cm^{-2} loading) of the total ink mass. The ionomer to catalyst ratio is 1:2. The suspension was ultra-sonicated until a stable suspension was reached.

Set-up

The electrolyte was 0.5 M sulfuric acid (ANALR grade or EMSURE Merck Millipore, as available to the project partners). All the measurements were performed in a glass jacket cell at $25 \text{ }^\circ\text{C}$ with a reversible hydrogen electrode (RHE) and a graphite counter electrode. The electrodes used had a glassy carbon disk with a platinum or gold ring.

The ring disk electrodes were polished and cleaned in an ultra-sonication bath with isopropanol and ultrapure water. The cleaned electrodes were dried in nitrogen and the ink applied to the surface and dried in an oven at $50 \text{ }^\circ\text{C}$, or at room temperature.

Break-in procedure

The activation of the catalyst was performed in O_2 -saturated electrolyte via cyclic voltammetry ($0.0 \text{ V} - 1.0 \text{ V}_{\text{RHE}}$, 10 mV s^{-1}) with a minimum of five cycles until the change in capacitance in the $0.95 - 1.0 \text{ V}_{\text{RHE}}$ region between two successive scans was less than 2 %.

ORR activity measurement and H_2O_2 formation

Cyclic voltammetry was performed in an O_2 -saturated electrolyte ($0.925 - 0.00 \text{ V}_{\text{RHE}}$, $1 - 2 \text{ mV s}^{-1}$, rotation 1600 rpm , ring potential $1.5 \text{ V}_{\text{RHE}}$) starting from open circuit potential (OCP) to the lower potential of $0.0 \text{ V}_{\text{RHE}}$ and a back scan to $0.925 \text{ V}_{\text{RHE}}$.

Accelerated stress test (AST)

The accelerated stress test was performed with a catalyst loading of 0.2 mg cm⁻² in sequence with the oxygen reduction reaction (ORR) activity measurement. The electrolyte was saturated with nitrogen and cyclic voltammetry applied (0.60 – 0.925 V_{RHE}, 100 mV s⁻¹, 10,000 cycles).

Data Analysis

For the determination of the kinetic current density j_{kin} the forward and backscan of the cyclic voltammetry of the disc current density were averaged to compensate for the capacitance, and the values of the current density j at 0.80 and 0.85 V_{RHE} and the diffusion limited current density j_{lim} at 0.20 V_{RHE} were determined. The Koutecký-Levich equation was used to calculate the kinetic current density at 0.80 and 0.85 V_{RHE}.

$$\frac{1}{j} = \frac{1}{j_{kin}} + \frac{1}{j_{lim}}$$
$$j_{kin} = \frac{j \cdot j_{lim}}{j_{lim} - j}$$

The following formula is used for the evaluation of the H₂O₂ production, with N as the collection efficiency of the ring-disk-electrode.

$$\%H_2O_2 = \frac{2 \cdot I_{Ring}/N}{I_{Disk} + I_{Ring}/N} \cdot 100$$

2.2 NITROGEN PHYSISORPTION

UNIPD: N₂ physisorption was performed in a Micromeritics Asap 2020 instrument. 100 to 150 mg of the catalyst material was inserted in a sample tube with glass wool and filling rods on top. Before the measurement, the samples were pretreated to remove any species adsorbed in and on the sample. The sample pretreatment consisted of heating the sample under vacuum (300 °C, 20 h). After cooling to room temperature, helium was backfilled into the sample tube. During the measurements, the sample was cooled to 77 K (liquid nitrogen). The N₂ physisorption test was operated under relative pressure p/p_0 in the range of 0 – 1. The Brunauer-Emmett-Teller (BET) equation was used to extract the surface area. Non-local density functional theorem (2D-NLDFT) was used for modeling isotherms in order to calculate pore size distributions of carbon microporous materials with pores from 0.35 to 25 nm. For the analysis an assumption of 2D model of finite slit pores having a diameter-to-width aspect ratio of 4-6-12 was made.

ICL: Nitrogen adsorption analysis was conducted on a Micromeritics Tristar II 3020. The analysis temperature was 77 K and the BET equation was used to extract the surface area. A molecular cross-sectional area of 0.1620 nm² for nitrogen was used. The best region for the linear fit was determined by the Rouquerol method. Samples were thoroughly degassed and dried overnight at 300 °C under nitrogen prior to the measurement. Gases used were nitrogen (BIP plus-X47S) for drying and adsorption and He (BIP plus-X47S) for the free space measurement, which was necessary for compensation of the sample

tube volume. Pore volume was determined as per NLDFT as implemented in the software Micromeritics “Microactive for Tristar II”. The model was based on slit shaped pores.

2.3 X-RAY PHOTOELECTRON SPECTROSCOPY

The measurements were carried out in a custom-designed UHV system equipped with an EA 125 Omicron electron analyser ending with a five channeltron detector, working at a base pressure of 10^{-10} mbar. The photoemission spectra were collected at room temperature using the Mg K α line ($h\nu = 1253.6$ eV) of a non-monochromatised dual-anode DAR400 X-ray source. The survey spectra were acquired using 0.5 eV energy step, 0.5 s collection time, and 50 eV pass energy; additionally single components (C 1s, O 1s, N 1s, Fe 2p $_{3/2}$) were acquired with the same parameters in order to increase accuracy of the calculation of surface composition (i.e. Fe 2p $_{3/2}$ line was acquired 60 times). High resolution spectra were acquired using 0.1 eV energy steps, 0.5 s collection time, and 20 eV pass energy for the curves fitting.

2.4 ^{57}Fe MÖSSBAUER SPECTROSCOPY

CNRS: ^{57}Fe Mössbauer spectra were measured with a Rh matrix ^{57}Co source. The measurements were performed keeping both the source and the absorber at room temperature. The spectrometer was operated with a triangular velocity waveform, and a gas filled proportional counter was used for the detection of the γ rays. Velocity calibration was performed with an α -Fe foil. The spectra were fitted individually with appropriate combinations of Lorentzian lines. In this way, spectral parameters such as the isomer shift (IS) and the electric quadrupole splitting (QS), and the relative resonance areas (A) of the different components were determined. Isomer shift values are reported relative to α -Fe.

UNIPD: Mössbauer spectroscopy was performed on a conventional constant acceleration spectrometer mounting a Rh matrix ^{57}Co source, nominal strength 1850 MBq. The spectra were fitted to Lorentzian line shapes with the minimum number of components. δ is reported relative to α -Fe foil. The spectrum recorded at 30 K was collected by using a close circuit ARS cryostat.

2.5 DYNAMIC LIGHT SCATTERING (DLS)

Particle size measurements were made using a dynamic light scattering (DLS) analyser (HPPS, Malvern Instruments Inc., Worcestershire, UK) with the Non-Invasive Backscatter optics (NIBS). Samples were prepared using approximately 1 mg of catalyst suspended in 30 mL of ethanol (>99.8% purity without denaturing additives). The suspension was then placed in an ultrasonic bath and sonicated for 1 hour. Prior to sample preparation, the stock ethanol solution was analysed by DLS to ensure it was free of particulates. Were any particulates be detected, the ethanol solution was filtered using a 0.2 μm syringe filter. A disposable PMMA cuvette was then filled with 2 mL of the catalyst suspension and placed in the HPPS analyser sample holder. The temperature was allowed to equilibrate at 25 °C for 10 minutes. Samples were then analysed using a collection time of 20 seconds. A total of 10 measurements were made

for each test and the tests were repeated 3 times. The number averaged particle diameter calculated for each of the 3 tests were then averaged.

2.6 CO-CHEMISORPTION

Measurement

CO pulse chemisorption and TPD were performed in a Thermo Scientific TPD/R/O 110 instrument. A mass of 100 to 150 mg of catalyst was inserted between two pieces of quartz wool at the bottom of the internal quartz bulb. Before the measurement, the catalyst was pretreated to remove any species strongly adsorbed on the metal-based sites on the surface, in particular O_2 . Pretreatment of the catalyst begins with cleaning of the lines with helium ($20 \text{ cm}^3/\text{min}$, 30 min) and a consecutive ramp heating from 30 to $600 \text{ }^\circ\text{C}$ ($10 \text{ }^\circ\text{C}/\text{min}$, 15 min hold time at $600 \text{ }^\circ\text{C}$) and followed by cooling to room temperature. Pulse chemisorption at $-80 \text{ }^\circ\text{C}$ (dry ice and acetone) consisted of 10 min line flushing (helium, $20 \text{ cm}^3/\text{min}$), followed by six CO pulses (helium as a carrier gas, $20 \text{ cm}^3/\text{min}$, loop volume was derived from c_f as 0.3277 ml) in intervals of 25 min. Prior to temperature programmed desorption (TPD) analysis, 3 consecutive CO pulses are performed to ensure the saturation of the active centers with CO. Thereafter TPD ($-80 \text{ }^\circ\text{C}$ to $600 \text{ }^\circ\text{C}$, $10 \text{ }^\circ\text{C}/\text{min}$, hold time 10 min, He as carrier, $20 \text{ cm}^3/\text{min}$) with a consecutive cooling to $30 \text{ }^\circ\text{C}$ ($20 \text{ }^\circ/\text{min}$) were performed.

CO Chemisorption analysis and evaluation of mass based site densities values

The turnover frequency (TOF) was evaluated under the assumption, that for one active metal- N_x centre on the surface, one CO molecule is adsorbed. At the chosen condition, the adsorption was assumed to be completed after three pulses. The last three CO pulses were used as the reference for the CO uptake calculations (figure 1).

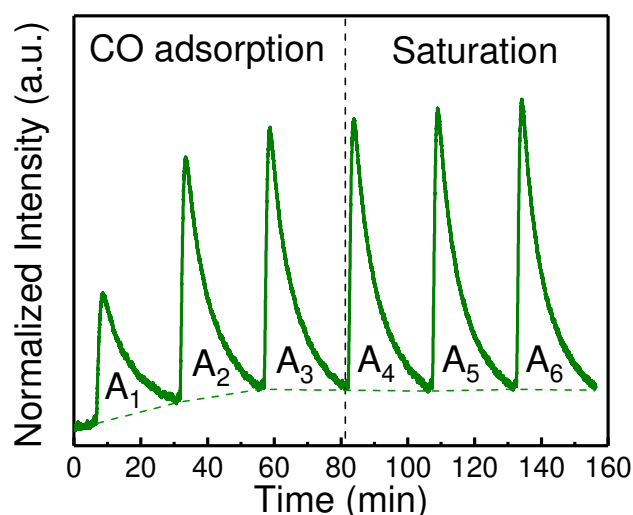


Figure 1: CO-pulse chemisorption on a Fe-N-C catalyst. Each peak indicates the non-adsorbed amount of CO gas. CO adsorption on the active centres is assumed to only take place in the first three pulses.

From the six consecutive CO pulses injected by the automated sample loop, the individual baseline-corrected integral pulse/peak areas $A_1 - A_6$ (formal units in mV s) were obtained and the differential peak

area ΔA , corresponding to the adsorbed molar CO amount was calculated. Assuming that CO adsorption has reached saturation after 3 pulses, ΔA can be obtained from

$$\Delta A = 6 \cdot \frac{A_{4,sample} + A_{5,sample} + A_{6,sample}}{3} - \sum_{k=1}^6 A_{k,sample}$$

Alternatively, if the adsorption process stretches over all six pulses the accurate value of ΔA can be obtained from

$$\Delta A = \sum_{k=1}^6 A_{k,calibration} - \sum_{k=1}^6 A_{k,sample}$$

Where $A_{k,calibration}$ are the integrated peak areas of individual consecutive sample loop CO pulses in absence of any adsorption (absence of catalyst). The average value of $A_{k,calibration}$, $\frac{\sum_{k=1}^6 A_{k,calibration}}{6}$, ranges around 32072 (dimensionless area). Using the average value of $A_{k,calibration}$ and the corresponding injected volume of CO, a calibration constant c_f can be derived (evaluated under typical lab conditions to be $c_f \approx 4.2 \cdot 10^{-7}$ mmol), which allows for the conversion between integral peak areas A and the corresponding injected molar amounts of CO.

Using this calibration constant c_f in combination with the differential integral peak area ΔA , the molar amount of adsorbed CO, $N_{CO,ad}$ was determined. The molar amount of adsorbed CO per mg catalyst, n_{CO} , was calculated by dividing by the mass of catalyst employed in the quartz tube of the chemisorption reactor:

$$N_{CO,ad} = c_f \cdot \Delta A \cdot 10^6 \text{ [nmol]}$$

$$n_{CO} = \frac{N_{CO,ad}}{m_{cat}} \text{ [nmol mg}_{cat}^{-1}]$$

The mass site density MSD_{CO} can be calculated via the Avogadro's constant N_A .

$$MSD_{CO} = n_{CO} \cdot N_A \cdot 10^{-6} \text{ [sites g}_{cat}^{-1}]$$

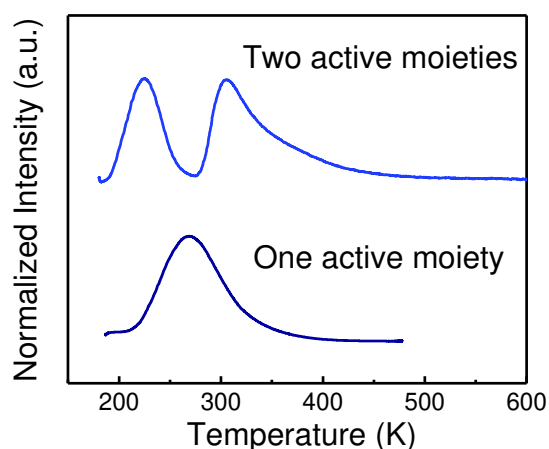


Figure 2: Temperature programmed desorption (TPD) of CO on non-PGM catalysts with two active centres (top) and one kind of active centre (bottom).

The TOF was calculated using the kinetic mass-based current activity at a given electrode potential, I_k (0.80 and 0.80 V_{RHE}), with units [mA/mg_{Cat}] and the catalyst mass-specific adsorbed molar amount of CO, n_{CO} (note that 1 mA = $10^{-3} \cdot N_A \cdot F^{-1}$ electrons s⁻¹)

$$TOF = \frac{I_k \cdot N_A}{MSD_{CO} \cdot F} = \frac{I_k \cdot N_A}{N_{CO} \cdot m_{Cat}^{-1} \cdot N_A \cdot 10^{-6} \cdot F} = \frac{I_k}{n_{CO} \cdot F} [electrons \text{ site}^{-1} \text{ s}^{-1}]$$

In the TPD, the temperature of desorption indicates the binding strength of the CO molecules. More than one peak indicates non-equivalent active centres in the Fe-N-C catalyst, (Figure 2).

2.7 NITRITE REDUCTION

Measurements are typically conducted with a conventional rotating ring disk electrode (Pine Instruments, model AFE6R1AU, with a mirror polished glassy carbon disk and rotator model AFMSRCE), where the catalyst is deposited on the glassy carbon disk. The loading is 0.2 mg cm⁻² and 0.5 M acetate buffer at pH 5.2 is utilised as electrolyte.

Figure 3 shows the steps necessary to collect the stripping data.

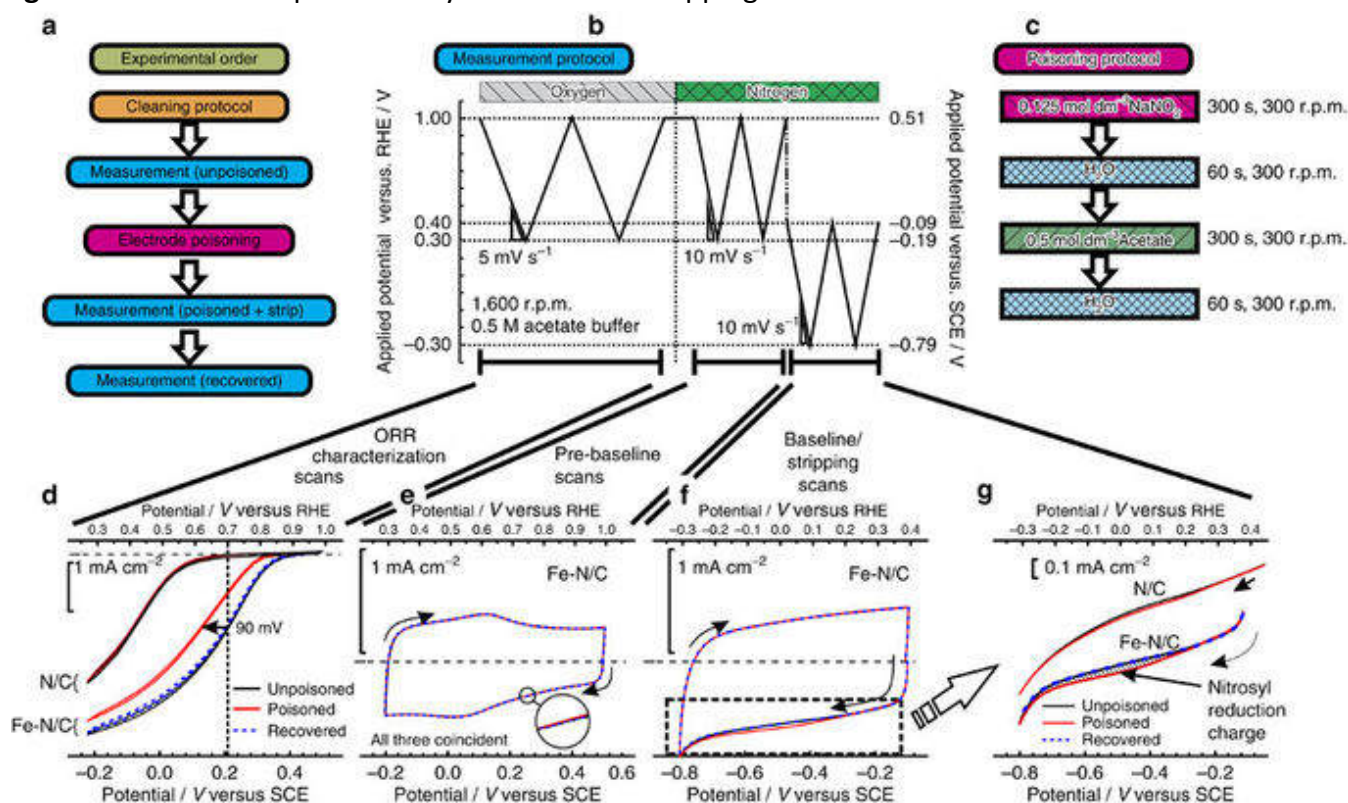


Figure 3: (a) Flow diagram showing steps used to assess the performance of a catalyst and determine the catalyst site density; (b) measurement protocol used to measure the electrochemical performance of the ORR and assess the charge associated with reductive stripping of the adsorbed nitrite; (c) protocol used to poison the electrode using a nitrite containing solution; (d) ORR performance of catalyst layer before, during and after nitrite adsorption; (e) wide range baseline scan (avoiding nitrite reduction area) for the catalyst layer before, during and after nitrite adsorption; (f) narrow baseline scan in the nitrite reductive stripping region before, during and after nitrite adsorption; (g) expansion of the region associated with nitrite stripping. All experiments were performed in a 0.5 M acetate buffer at pH 5.2 for Fe-N/C catalyst using a rotating disk electrode setup; loading 0.27 mg cm⁻².

In summary, it consists of measuring the background capacitive current and kinetic activity, then poisoning the catalyst, measuring the poisoned activity, stripping off the poison and verifying that the activity is returned to the baseline.

Figure 4 shows the extraction of stripping charge from the capacitive background scan and correlation with kinetic current before and after poisoning. From these data the site density and turnover frequency can then be estimated.

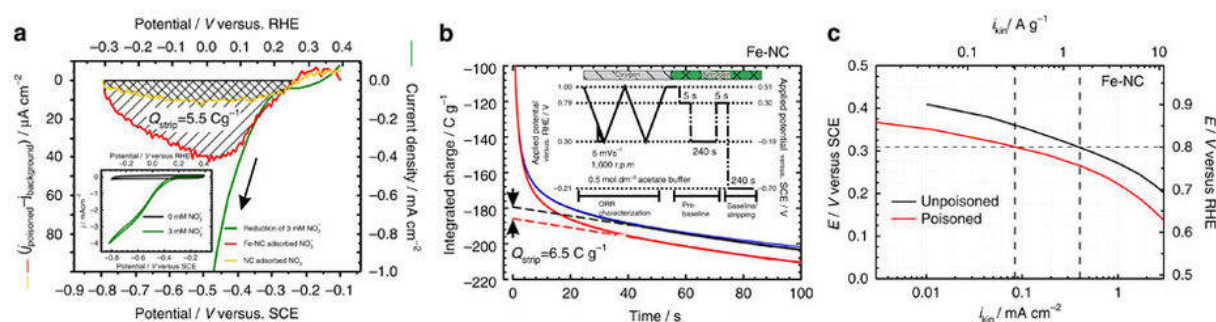


Figure 4: (a) Comparison between homogeneous reduction of aqueous nitrite (3 mM NaNO₂ in acetate buffer), and excess current associated with reductive stripping of intermediate on Fe-N/C or N/C catalyst. The reductive stripping curve is produced by subtracting the unpoisoned from poisoned curve in Fig. 3g. Inset is the complete nitrite reduction curve for homogeneous nitrite in solution. (b) Chronoamperometric transients for determination of the reductive stripping charge for the Fe-N/C catalyst; (c) kinetic current density of Fe-N/C catalyst before and after the poisoning step. O₂-saturated electrolyte, 5 mV s⁻¹ background and iR-corrected rotating disk electrode experiments at 1,600 rpm, electrolyte: 0.5 M acetate buffer, loading: 0.27 mg cm⁻².

3. RESULTS AND DISCUSSION

3.1 ELECTROCHEMICAL MEASUREMENTS – SD AND TOF

The measurements of the catalyst in RRDE setup is the first step in determining the catalytic activity and the selectivity in terms of hydrogen peroxide production. The kinetic current at different potentials was determined and used to calculate the turnover rate from the site density, which was evaluated from *in situ* nitrite reduction and *ex situ* CO-chemisorption.

Electrochemical data

The RRDE experiments were performed on two different catalyst loadings on the disk, at 0.2 and 0.8 mg cm⁻². Figure 5 shows an example of polarisation curves of the tested catalysts at the higher loading. Measurements were made on catalyst 1 before and after ball milling. The smaller particle size (see Figure 11) appeared to influence the performance of the catalyst in RRDE testing. Figure 6 shows the production of hydrogen peroxide in the potential range from 0.00 – 0.85 V_{RHE}.

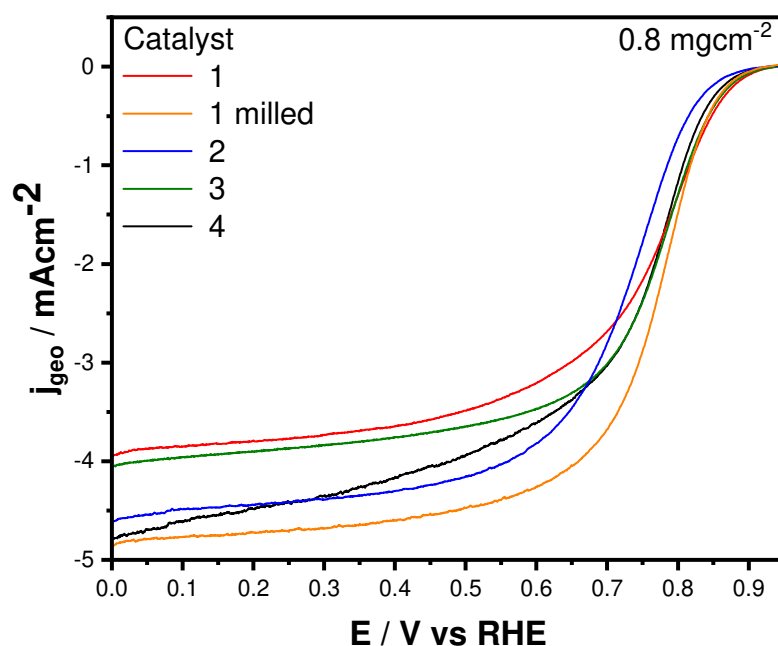


Figure 5: Example of polarisation curves of the catalysts in saturated oxygen in 0.5 M H₂SO₄ and a catalyst loading of 0.8 mg cm⁻².

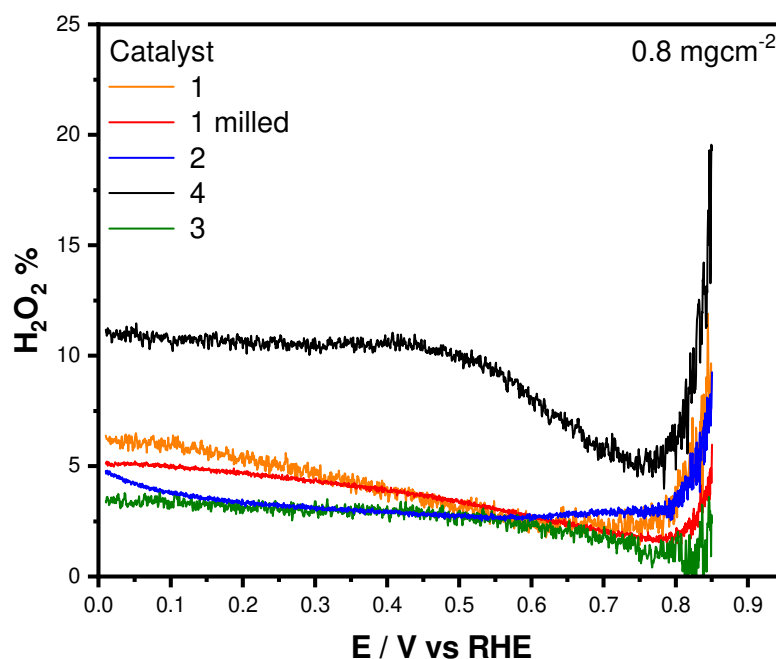


Figure 6: Example of determined H₂O₂ production of the tested catalysts in saturated oxygen in 0.5 M H₂SO₄ and a catalyst loading of 0.8 mg cm⁻².

Table 2 and Table 3 show the values averaged values of the main electrochemical data with their corresponding errors. Each catalyst was measured in at least two different laboratories with two to three repetitions for each catalyst and loading.

Table 2: Electrochemical metrics at catalyst loading of 0.2 mg cm⁻² before and after accelerated stability testing.

0.2 mg cm ⁻² Catalyst	Initial – Before AST					Final – After AST				
	J _{Lim}	J _{Kin}	J _{Kin}	H ₂ O ₂	H ₂ O ₂	J _{Lim}	J _{Kin}	J _{Kin}	H ₂ O ₂	H ₂ O ₂
	(0.2 V _{RHE}) [mA cm ⁻²]	(0.80 V _{RHE}) [mA cm ⁻²]	(0.85 V _{RHE}) [mA cm ⁻²]	(0.2 V _{RHE}) [%]	(0.7 V _{RHE}) [%]	(0.2 V _{RHE}) [mA cm ⁻²]	(0.80 V _{RHE}) [mA cm ⁻²]	(0.85 V _{RHE}) [mA cm ⁻²]	(0.2 V _{RHE}) [%]	(0.7 V _{RHE}) [%]
1	3.5 ± 0.3	0.40 ± 0.09	0.12 ± 0.06	5 ± 2	5 ± 3	3.1	0.4	0.09	10 ± 2	14 ± 3
2	4.77 ± 0.07	0.24 ± 0.06	0.05 ± 0.02	8 ± 6	14 ± 9	4.2 ± 0.2	0.22 ± 0.01	0.05 ± 0.01	8 ± 6	20 ± 13
3	4.3 ± 0.6	0.465 ± 0.005	0.100 ± 0.001	6 ± 4	7 ± 3	3.9 ± 0.5	0.18 ± 0.07	0.04 ± 0.02	7 ± 3	19 ± 6
4	3.9 ± 0.7	0.48 ± 0.43	0.10 ± 0.09	7 ± 5	8 ± 5	3.41 ± 0.09	0.13 ± 0.05	0.03 ± 0.01	10	16

Table 3: Electrochemical metrics at catalyst loading of 0.8 mg cm⁻².

0.8 mg cm ⁻² Catalyst	Initial – Before AST				
	J _{Lim}	J _{Kin}	J _{Kin}	H ₂ O ₂	H ₂ O ₂
	(0.2 V _{RHE}) [mA cm ⁻²]	(0.80 V _{RHE}) [mA cm ⁻²]	(0.85 V _{RHE}) [mA cm ⁻²]	(0.2 V _{RHE}) [%]	(0.7 V _{RHE}) [%]
1	4.3 ± 0.5	1.8 ± 1.0	0.5 ± 0.3	5 ± 4	4 ± 6
2	4.41 ± 0.03	0.81 ± 0.01	0.18 ± 0.01	3.0 ± 0.3	3.4 ± 0.6
3	4.4 ± 0.5	2.6 ± 0.7	0.7 ± 0.2	2.6 ± 0.6	1.9 ± 0.3
4	4.9 ± 0.3	2.1 ± 1.2	0.4 ± 0.2	5 ± 4	3 ± 2

Table 4: Initial mass based kinetic current at the two different loadings and potentials shows the comparison of mass based current for each catalyst at the loadings of 0.2 and 0.8 mg cm⁻². Due to the error margin, a comparison of the catalysts is not easily achievable. Catalyst 3 shows highest and most stable kinetic current at all potentials and catalyst loadings. Catalyst 1 and 4 show values in the same range. Catalyst 2 is the least active.

Table 4: Initial mass based kinetic current at the two different loadings and potentials

Catalyst	J _{Kin,mass} 0.80 V _{RHE}		J _{Kin,mass} 0.85 V _{RHE}	
	0.2 mg cm ⁻²	0.8 mg cm ⁻²	0.2 mg cm ⁻²	0.8 mg cm ⁻²
	[mA mg ⁻¹]	[mA mg ⁻¹]	[mA mg ⁻¹]	[mA mg ⁻¹]
1	2.0 ± 0.4	2.2 ± 1	0.6 ± 0.3	0.7 ± 0.4
2	1.2 ± 0.3	0.7 ± 0.5	0.26 ± 0.09	0.22 ± 0.01
3	2.33 ± 0.02	3.2 ± 0.9	0.496 ± 0.003	0.9 ± 0.3
4	2.4 ± 2	2.60 ± 1	0.5 ± 0.5	0.6 ± 0.2

The influence of ball milling on catalyst 1 is shown in Figure 5Figure 6 for the polarisation curve and peroxide production. While the peroxide production slightly decreased after ball milling, the diffusion limited current drops significantly. The determined mass based currents can be seen in Table 5, and differ slightly for unmilled and milled catalyst.

Table 5: Comparison of Initial mass based kinetic current of catalyst 1 as obtained and after ball milling.

Catalyst	$J_{\text{Kin, mass}} 0.80 \text{ V}_{\text{RHE}}$		$J_{\text{Kin, mass}} 0.85 \text{ V}_{\text{RHE}}$	
	0.2 mg cm ⁻²	0.8 mg cm ⁻²	0.2 mg cm ⁻²	0.8 mg cm ⁻²
	[mA mg ⁻¹]	[mA mg ⁻¹]	[mA mg ⁻¹]	[mA mg ⁻¹]
1	2.0 ± 0.4	2.2 ± 1	0.6 ± 0.3	0.7 ± 0.4
1' (milled)	1.9	2.6	0.4	0.5

Site density and turnover frequency

In situ nitrite reduction and *ex situ* CO-chemisorption, were used to determine the site density and the turnover frequency. An example for the evaluation of the site density via nitrite reduction is provided in Figure 7 and an example of CO-chemisorption in Figure 8.

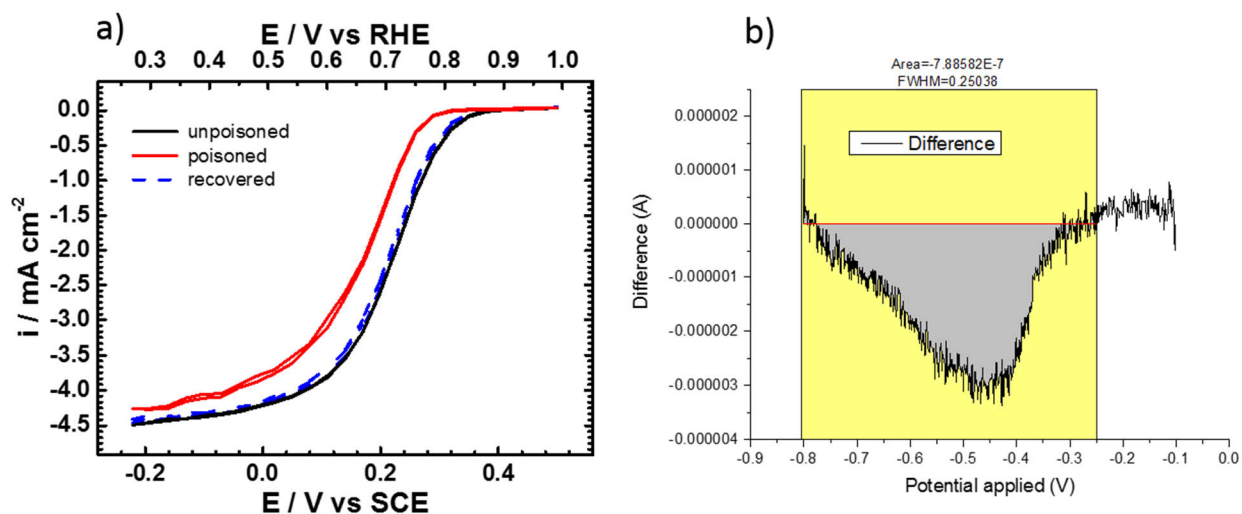


Figure 7: An example of nitrite stripping as per the procedure described in 2.3.7. (a) ORR activity of catalyst layer before, during and after nitrite adsorption (b) excess current associated with reductive stripping of nitrite used to determine the active site density.

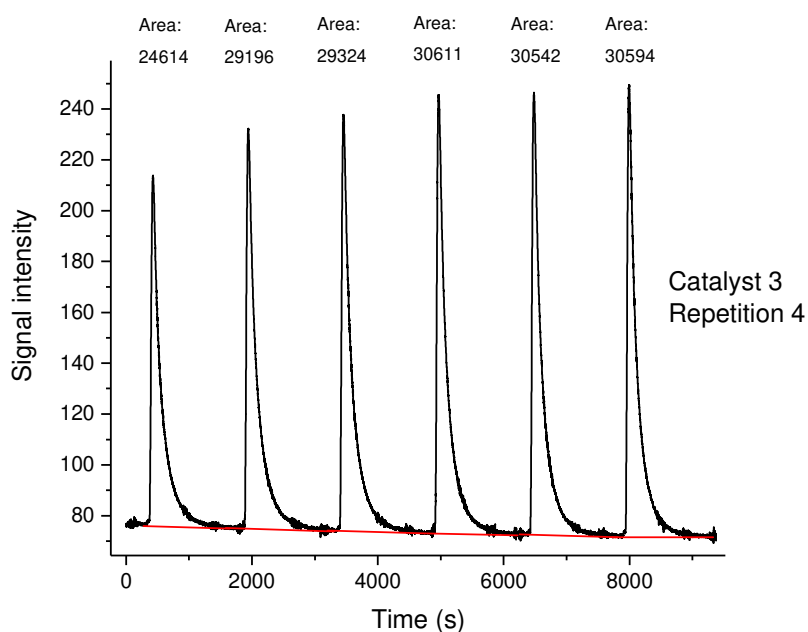


Figure 8: Example of CO chemisorption on catalyst 3 with the shown integrated dimensionless areas.

The site density values differ in the two methods, as expected, with that determined from CO-chemisorption being systematically higher. The active centres using *in situ* nitrite reduction method are not as easily accessible and the pore structure is possibly flooded with electrolyte. The gaseous carbon monoxide used in the *ex situ* method of CO-chemisorption has a better accessibility to active centres in the pore structures of the catalysts. Another explanation could be different selectivity of nitrite and CO on various Fe moieties present in differing surface concentrations in each of the catalysts due to the variety of conditions used in the catalyst syntheses

Regardless, the turnover frequency was evaluated using the averaged mass based kinetic current at 0.80 and 0.85 V_{RHE} from table 4.

Table 6: Site density and turnover frequency as evaluated by nitrite reduction and CO chemisorption measurements.

Catalyst	Method	Site density [10^{19} sites g^{-1}]	Turnover frequency	
			0.80 V_{RHE} [electrons sites $^{-1}$ s $^{-1}$]	0.85 V_{RHE} [electrons sites $^{-1}$ s $^{-1}$]
1	Nitrite reduction	2.73	0.43	0.12
	CO Chemisorption	5.80 \pm 0.08	0.20	0.06
2	Nitrite reduction	0.86	0.96	0.34
	CO Chemisorption	2.20 \pm 0.6	0.41	0.08
3	Nitrite reduction	0.25	7.23	0.80
	CO Chemisorption	2.02 \pm 0.03	0.71	0.16
4	Nitrite reduction	0.63	3.45	0.46
	CO Chemisorption	3.12 \pm 0.2	0.47	0.10

Figure 9 shows the site density comparison of the two catalysts. All the catalysts have SDs in the range of 10^{19} sites g^{-1} , both methods show that catalyst 1 has the highest SD. For the other catalysts the ranking for both methods differs. For the CO chemisorption method the second highest SD is seen with catalyst 4. Catalyst 2 and 3 are considered to have equally high SDs. For nitrite reduction method the ranking is from catalyst 2 with the second highest SD, to catalyst 4 and catalyst 3 with the lowest SD.

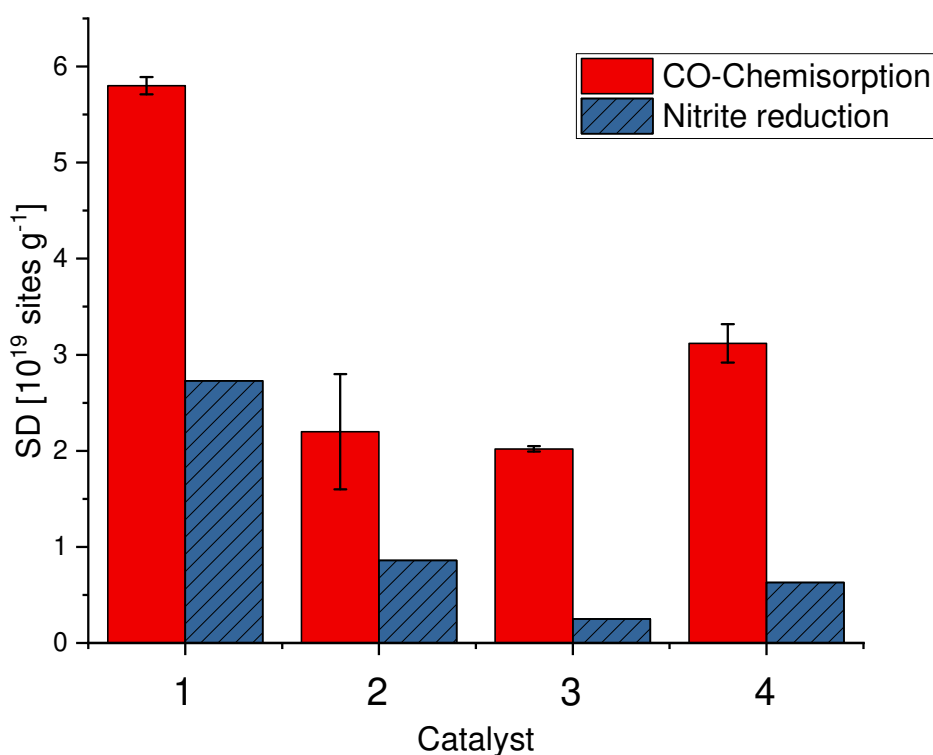


Figure 9: Site density by CO-chemisorption and nitrite reduction.

Figure 10: shows the calculated turnover frequency for the benchmark catalysts for the kinetic current at the two different potentials. The range of the TOF is from 0.06 up to 7.23 electrons $\text{s}^{-1} \text{g}^{-1}$. The TOF trend for both determination methods is the same, with catalyst 3 as the most active, followed by 4, 2 and 1. The nitrite reduction gave exceptionally high values for catalysts 3 and 4. A correlation with site density shows that catalyst 1 with the highest SD has the lowest turnover frequency.

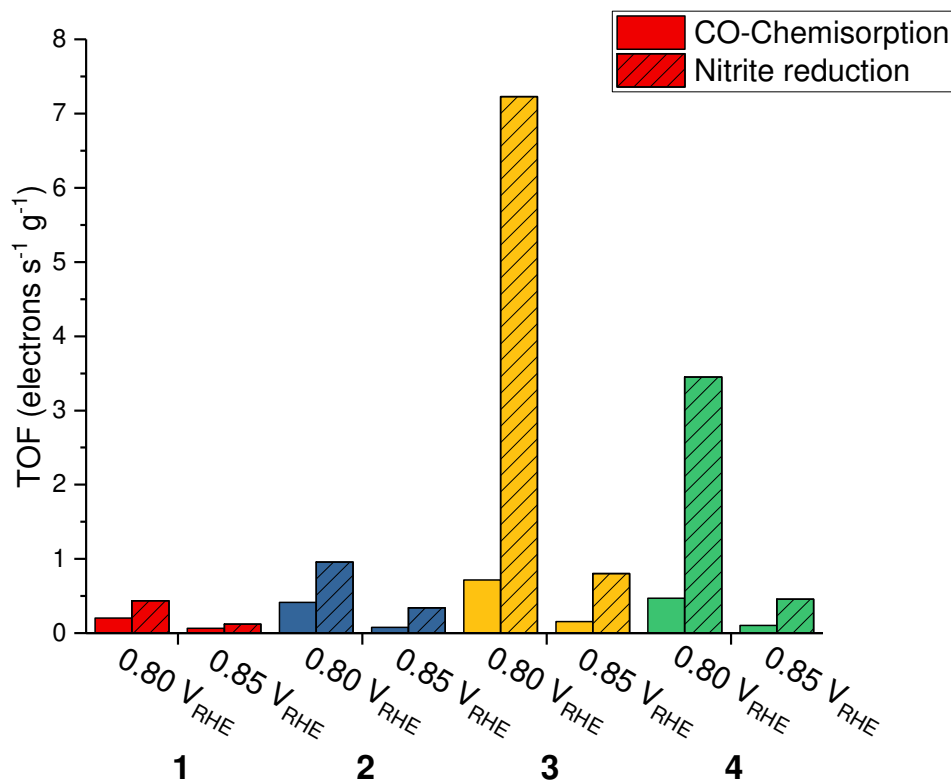


Figure 10: Turnover frequencies at 0.80 and 0.85 V_{RHE} obtained from the combination of j_{kin} measured by RDE and site density measured either with CO chemisorption or nitrite reduction.

3.2 PHYSICOCHEMICAL CHARACTERISATION

Dynamic light scattering (DLS)

The number averaged particle size, d_{av} , for each of the four benchmark catalysts as measured by DLS is shown in Figure 11. The asymmetry around the intensity peak towards larger particle size of the size distributions, consistently observed among all four benchmark catalysts, can qualitatively be attributed to the tendency of carbon particles to aggregate into micrometric particles during high temperature pyrolysis as well as in dispersions of various solvents. No obvious trend correlating the DLS measured particle size to catalyst specific surface area measured by N₂ adsorption (Table 13) was found, nor was any clear trend in the electrochemical activity, specifically in the mass transfer region of the ORR polarisation curves, observed between the different benchmark catalysts based on DLS measured particle size. This is likely due to a large variety in synthetic technique, composition, and morphology (among other factors) of the different benchmark catalysts.

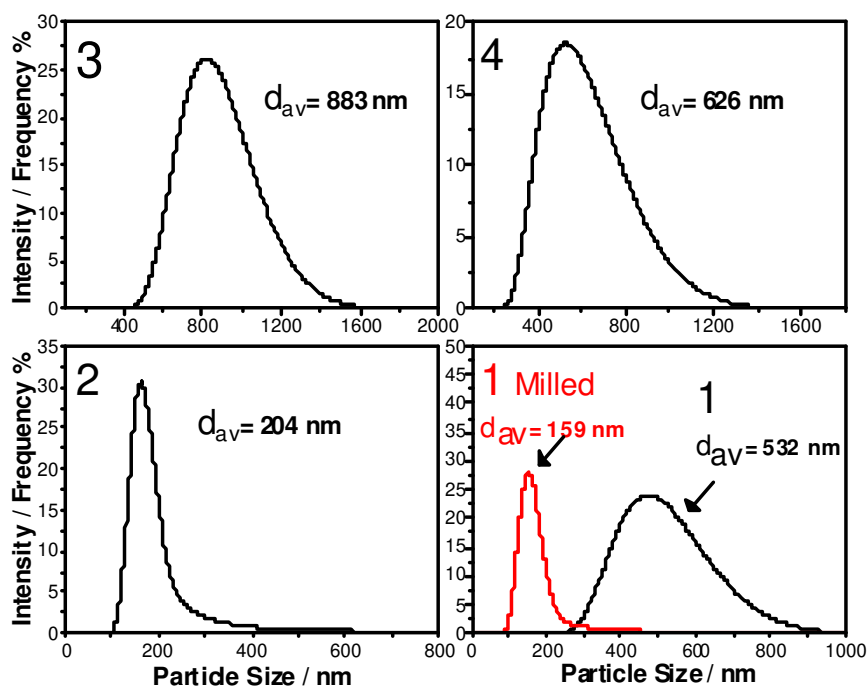


Figure 11: Number averaged particle size (d_{av}) distributions for the four benchmark catalysts measured by DLS. Figures on the lower right shows the size distributions for the catalyst 1, with and without ball milling (catalyst 1 milled).

To explore the effect of catalyst ball milling prior to RRDE ink preparation, catalyst 1 was arbitrarily selected for analysis. Inks were prepared using catalyst 1 with and without prior ball milling, milling performed in a slurry of water and IPA, and drop-cast on glassy carbon ring-disc electrodes with a loading of $800 \mu\text{gcm}^{-2}$. It was found that no significant gain in the mass transfer corrected kinetic current density could be obtained from catalyst milling, where i_k at 0.8 V vs. RHE measured with and without catalyst milling were 2.58 and 2.42 mAcm^{-2} (measured by CNRS) respectively. However, a significant improvement in the diffusion-limited current density was observed after ball milling, an improvement from 3.80 to 4.73 mA cm^{-2} (measured by CNRS) at 0.2V vs. RHE. DLS measurements on catalyst 1 show an average particle size of 532 nm prior to ball milling and a 3-fold reduction in average particle size, 159 nm, measured after ball milling (Figure 11 lower right). Comparing catalyst 1 prior to ball milling to other benchmark catalyst, catalyst 3 and 4 show a trend of reaching a higher diffusion-limited current density than catalyst 1, despite the DLS measured particle size of these catalysts being larger than that of catalyst 1. After ball milling, catalyst 1 reaches a diffusion-limited current density greater than that of catalysts 3 and 4. Therefore, in the future activity measurements made by RRDE techniques, the effects of ball milling prior to ink preparation should be investigated as this effect may vary depending on the specific morphology and composition of each catalyst.

TPD

The temperature programmed desorption measurements show the relative intensity of desorbed gas from the sample. The measurements start from a CO-saturated state at -80 °C up to the maximum temperature of 600 °C. The catalysts show all two major desorption maxima (Figure 12), one in the region of -52 °C and one in the region of 20 °C and indicates different iron moieties with varying adsorption strength (Table 7). The close proximity of the desorption maxima of the four catalysts could be explained by the existence of similar iron moieties, especially in the first maximum around -52 °C. The second maximum differs more between the catalyst, as well as the relative intensity of both the maxima.

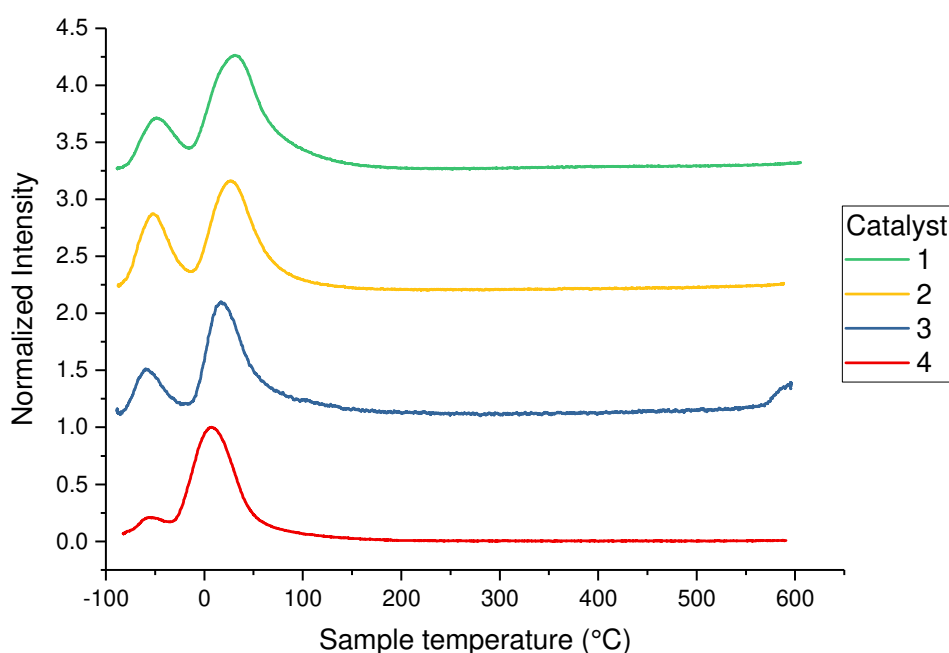


Figure 12: Example of each temperature programmed desorption of CO gas from the catalysts.

Table 7: Desorption signal maxima in temperature programmed desorption.

Catalyst	1. Desorption maximum [°C]	2. Desorption maximum [°C]
1	-48 ± 2	31 ± 4
2	-50 ± 2	34.0 ± 11
3	-55 ± 2	17 ± 2
4	-55 ± 2	8 ± 4

Mössbauer spectroscopy

The four catalysts present different overall Mössbauer spectra (Figure 13). Catalyst 3 shows only the presence of two doublets (assigned to atomically dispersed iron coordinated with nitrogen atoms). Catalyst 4 show, in addition, the presence of a minor singlet assigned non-magnetic γ -Fe or to nanosized superparamagnetic α -Fe. Catalyst 1 shows, in addition to D1, D2 and the same singlet component, a small

contribution of a sextet component that is unambiguously assigned to magnetic α -Fe. Catalyst 3 has an overall spectrum different from the others, with a main fraction of the singlet component, and doublets that are less well defined (broader) than in the other catalysts.

Table 8: Relative fraction of each spectral component in the catalysts, as derived from the fitting of their ^{57}Fe Mössbauer spectra. The spectra were measured at room temperature.

Spectral component →	D1	D2	α -Fe	γ -Fe	Fe_3C
Catalyst ↓	% area of absorption due to each spectral component				
1	42	26	18	10	3
1'	-	-	-	-	-
2	38	62	0	0	0
3	11	43	9	35	2
4	40	49	0	11	0

Table 9: Isomer shift of each spectral component in the catalysts, as derived from the fitting of their ^{57}Fe Mössbauer spectra. The spectra were measured at room temperature.

Spectral component →	D1	D2	α -Fe	γ -Fe	Fe_3C
Catalyst ↓	Isomer shift value of each component / mm s^{-1}				
1	0.34	0.45	0	-0.08	0.185
1'	-	-	-	-	-
2	0.36	0.55	-	-	-
3	0.37	0.40	0	-0.12	0.12
4	0.36	0.41	-	-0.08	-

Table 10: Quadrupole splitting, QS, or hyper-fine field, H, values of the doublet D1 and D2 and sextet components (α -Fe and γ -Fe), respectively, as derived from the fitting of the ^{57}Fe Mössbauer spectra of the catalysts. The spectra were measured at room temperature.

Spectral component →	D1	D2	α -Fe	γ -Fe	Fe_3C
Catalyst ↓	QS or H value / in units of mm s^{-1} or Tesla, respectively				
1	1.03	2.48	33	-	20
1'	-	-	-	-	-
2	0.96	2.20	-	-	-
3	0.75	2.34	33.2	-	20.8
4	1.10	2.77	-	--	-

Despite different overall shapes of the spectra, the fitting of the spectra with unconstrained parameters resulted in spectral components with relatively common parameters among these four catalysts. As can be seen in Table 8 – 10, the isomer shift and quadrupole splitting of the doublet with small QS value

(labelled D1) ranges only from 0.34-0.37 mm s⁻¹ and 0.75-1.10 mm s⁻¹, respectively. While some small differences in exact Fe coordination of “D1” in these different catalysts probably exist, it nevertheless clearly makes sense to assign this spectral component to a single generic type of Fe ion coordination to discuss the results obtained with these different catalysts. In the literature, D1 has often been assigned to a Fe(II)-N₄ square-planar (or near square planar) configuration with zero-spin, as per analogy of the Mössbauer response of FeN₄ square planar macrocycles (unpyrolysed reference materials). The doublet with larger QS-value has also relatively narrow range of isomer shift and quadrupole splitting value among these four catalysts (Table 9, Table 10), and has often been assigned to either distorted Fe(II)N₄ in medium spin state (S=1) or Fe(III)N₄ in high spin state. Coupling of Mössbauer with other characterisation methods (XPS, magnetic measurements, etc.) will however be necessary for supporting the latter assignments more clearly.

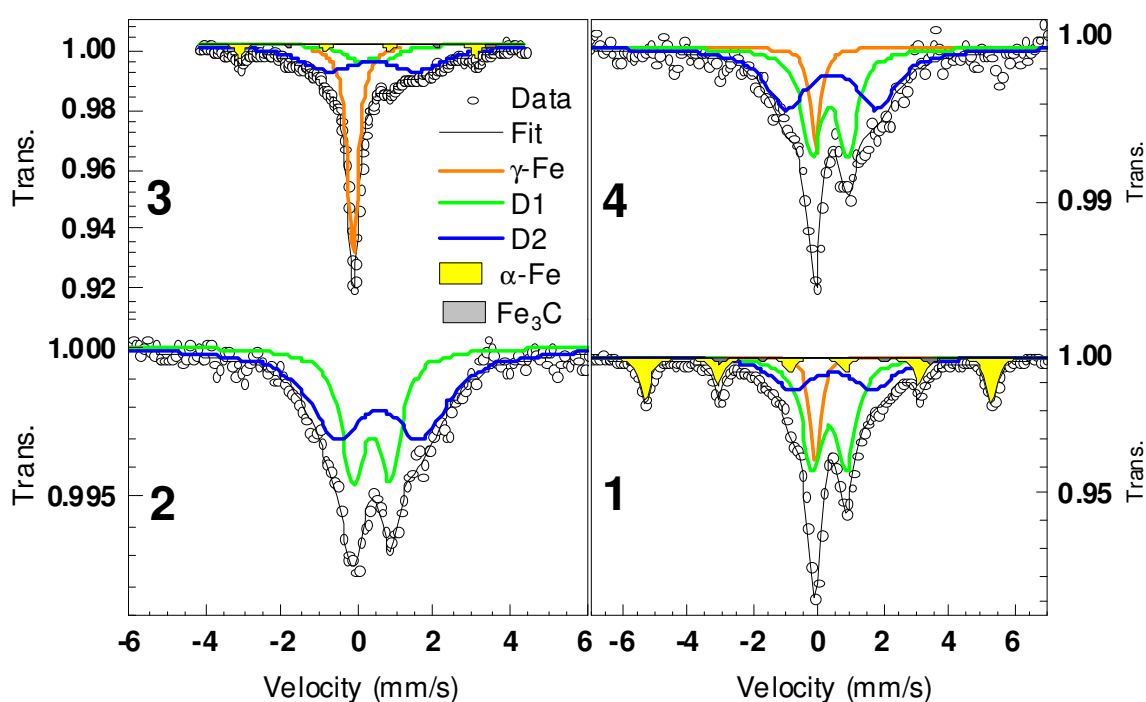


Figure 13: Comparison of the ⁵⁷Fe Mössbauer spectra of the four benchmarking catalysts. The spectra were recorded at room temperature. The coloured curves represent the fitted position and intensity for each individual spectral component.

While the singlet component has an isomer shift value corresponding either to nano-sized α -Fe or to non-magnetic γ -Fe, the measurement at low temperature of catalyst 3 shows that the singlet did not split into a sextet at 30 K, and this thereby excludes the possibility for assignment to nanosized superparamagnetic γ -Fe (nano- α -Fe becomes magnetically ordered at 30 K).

For the sextets, the isomer shift and hyperfine field values derived from the fittings correspond perfectly to those for the reference compounds α -Fe and Fe₃C, so that those assignments are completely unambiguous. The advantage of Mössbauer spectroscopy compared to XRD for those phases is however the possibility to identify clearly very small amount of such phases, which would not be possible with XRD (broad peak with too low intensity relative to noise background).

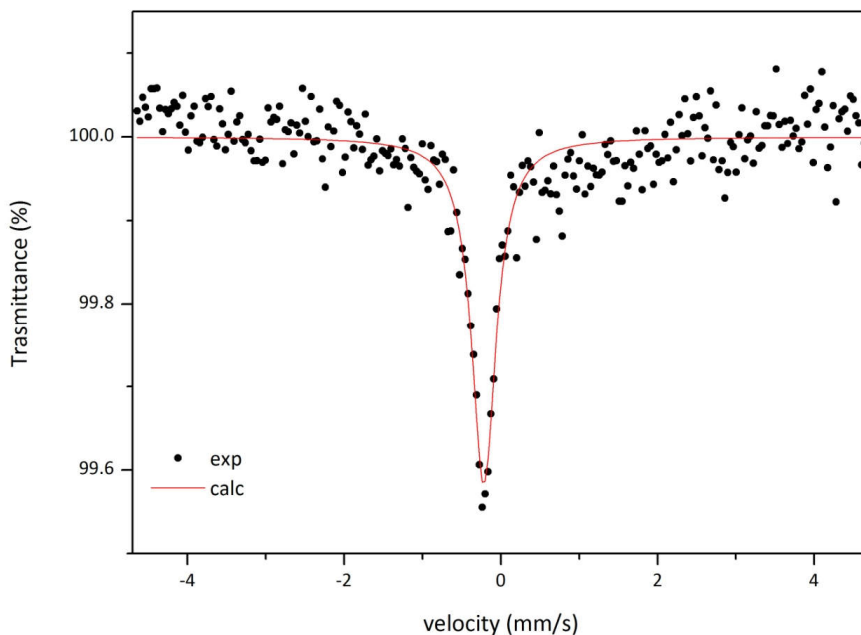


Figure 14: ^{57}Fe Mössbauer spectrum of catalyst 3 measured at room temperature (the higher noise is due to smaller amount of sample used here relative to that in Figure 13).

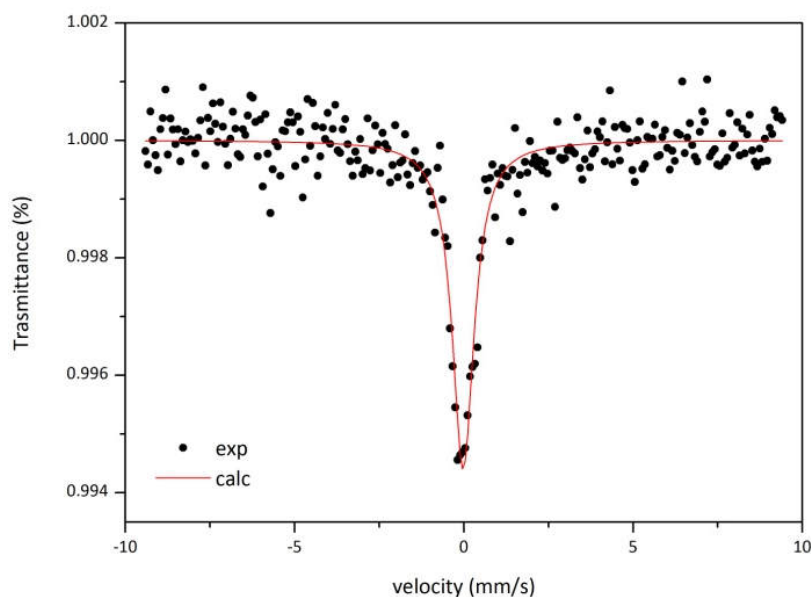


Figure 15: ^{57}Fe Mössbauer spectrum of catalyst 3 measured at 30 K (the higher noise is due to smaller amount of sample used here relative to that in Figure 13). The data shows the singlet component was unmodified at 30 K relative to room temperature.

X-ray photoelectron spectroscopy (XPS)

The Fe_{2p} XPS data has low precision, because the signal intensity of Fe is close to the detection limit and the final spectra have a very low signal/noise ratio. This is usual for Fe-N-C catalysts, due to the low site density of atomically dispersed FeN_4 -type sites. XPS at Fe_{2p} level gives however an estimation of the Fe amount located on or near the surface (first few nm from surface), and this can be useful to distinguish such Fe amount from those that would be encapsulated in very thick layers of carbon (> 10 nm), which would be invisible by XPS.

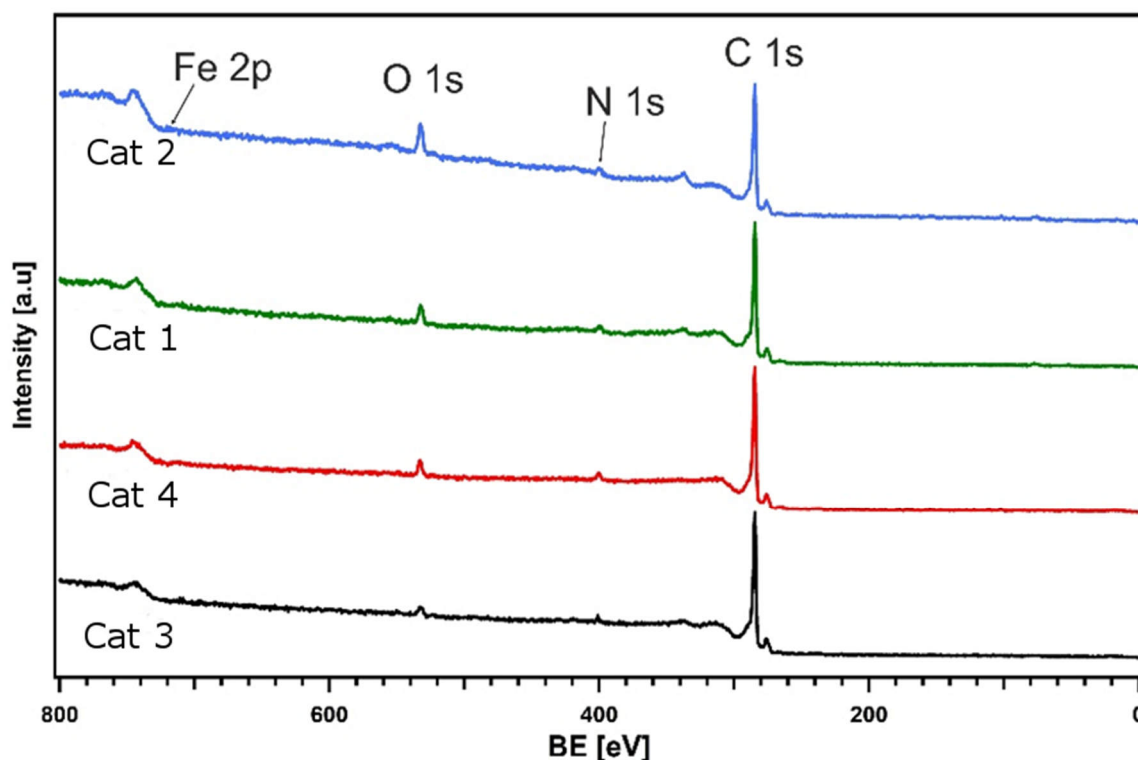


Figure 16: XPS survey spectra of catalyst samples.

In contrast, the N 1s region is richer and gives more diagnostics on the content but also speciation of nitrogen groups and N-Fe coordination. However, the detailed procedure for fitting the N1s spectra in such materials, and the assignments of the specific binding energies, is still a topic of intense research and variability across laboratories and over time. The assignment and identification of N-Fe coordination in particular is difficult, as it requires the knowledge of the exact coordination of such active sites (coordination number of Fe with N varying from 2 to 4, second coordination sphere with 8, 10 or 12 carbon atoms, pyrrolic or pyridinic type nitrogen, etc), a research topic in itself. Due to these difficulties, in many studies the N_x -Fe components are not distinguished from simpler nitrogen groups not coordinated to Fe. Considering the close value of the binding energies of the different N_x -Fe components adopted in literature, we retained here a conservative fitting procedure to avoid data over-interpretation.

Table 11: Surface composition (at.%) of the catalyst samples.

	C 1s	O 1s	N 1s	Fe 2p _{3/2}
1	91.51	5.98	2.15	0.36
2	86.78	9.99	3.06	0.16
3	95.43	2.01	2.30	0.25
4	91.46	4.91	3.37	0.26

Figure 17 shows the N 1s XPS spectra for the four samples, fitted with the model reported in Ref. [1], i.e. assigning one component to N_x-Fe coordination (x possibly from 2 to 4). The peak at the lowest BE 397.8 eV can be assigned to imine or cyano groups while the peak at 398.8 eV is due to pyridinic nitrogen and metal coordinated to nitrogen in disordered states such as N₂-Fe and N₃-Fe.

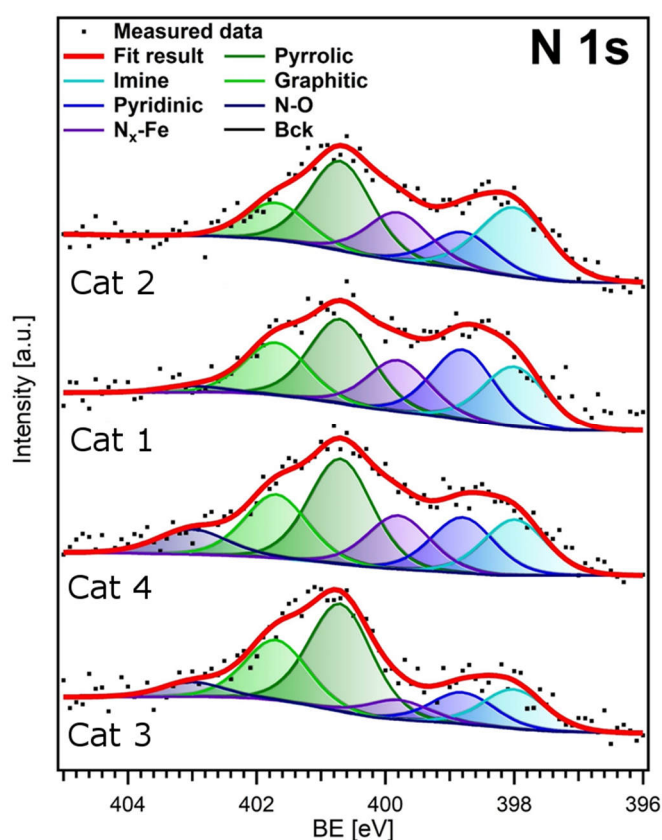


Figure 17: High resolution N 1s XPS spectrum for benchmark samples.

The peak at 399.9 eV in the metal-free samples has contribution to amine group, whereas in the case of Fe-containing samples, it is assigned to iron coordinated to nitrogen groups in a mesomeric N₄-Fe configuration. The peaks at 400.7 eV, 401.7 eV and 402.7 eV correspond to pyrrolic, graphitic and N-O

nitrogen, respectively. The results of the fitting procedure are reported in Table 12. The corresponding analysis of the deconvoluted components is given in table 12.

Table 12: Fraction of the different N species present in the catalyst samples.

Catalyst	N imine (%) (397.8 eV)	N Pyridinic (%) (398.8 eV)	N N _x -Fe (%) (399.9 eV)	N Pyrrolic (%) (400.7 eV)	N Graphitic (%) (401.7 eV)	N N-O (%) (402.7 eV)
1	18.6	21.6	15.8	25.9	16.2	1.9
2	26.6	12.8	16.7	31.0	12.9	-
3	14.4	11.6	7.1	39.4	22.1	5.4
4	15.3	15.4	14.8	29.1	17.6	7.8

N₂ physisorption

All the samples showed very high BET surface area and isotherms with well-defined hysteresis indicating the presence of mesopores. Catalyst 1 showed the highest BET surface area for the most part due to micropores, followed by catalyst 4, which conversely has pores especially in the mesopore range. Catalyst 3 ranked in the middle showing a very high mesopore volume whereas catalyst 2 shows a balance between micro and mesopores.

Table 13: BET surface area and pore volumes calculated from N₂ adsorption isotherms.

Catalyst	Measured by	BET	V _{micro}	V _{meso}	V _{TOT}
		m ² g ⁻¹	cm ³ g ⁻¹	cm ³ g ⁻¹	cm ³ g ⁻¹
1	Lab 1	814	0.196		
	Lab 2	866	0.269	0.203	0.472
2	Lab 1	475	0.123		
	Lab 2	450	0.137	0.317	0.454
3	Lab 1	621	0.106		
	Lab 2	565	0.103	0.92	1.023
4	Lab 1	775	0.145		
	Lab 2	750	0.181	0.88	1.061

Catalyst 1: Isotherm III / IV(a), in particular Type III is given by finite amount adsorbed at the saturation pressure. The hysteresis loop is H2(a) / H4. H2(a) loops is for instance given by ordered mesoporous material, this characteristic can be attributed either to pore-blocking/percolation in a narrow range of pore necks or to cavitation-induced evaporation.

Catalyst 2: Isotherm II / IV(a) is given by mesoporous adsorbent, in particular there is a distinctive sharp knee, which corresponds to the completion of monolayer coverage. The thickness of the adsorbent multilayer appears to increase when $p/p_0 = 1$. The hysteresis loop can be considered H3 / H4, where the pronounced uptake at low range is associated with filling micropore. H3 loop resembles the adsorption branch of Type II isotherm, loops of this type are given by non-rigid aggregates of plate-like particle.

Catalyst 3: Isotherm IV(a), with a medium hysteresis loop between H2(b) and H3. Complex pore structure and network effect are important. H2(b) profile is due to pore blocking, the neck widths is much larger because of mesocellular silica foam or meso-ordered silica after hydrothermal treatment. Instead, H3 probably is due to the presence of macropores, which are not completely filled with pore condensate.

Catalyst 4: Isotherm IV(a), with a hysteresis loop of H2(b). The isotherm profile is similar to that of catalyst 3. The synthetic approach for preparation of catalyst 4 is based on fumed silica Cab-O-Sil that affords a mesoporous carbon structure, which has this isotherm profile.

4. CONCLUSIONS AND FUTURE WORK

The benchmarking study was performed in order to evaluate the performance of four state of the art non-PGM catalysts. The measuring protocols will be further used for the evaluation of novel catalysts, developed in CRESCENDO. Dynamic light scattering, XPS, Mössbauer spectroscopy and nitrogen physisorption were used to characterise the samples. The key metrics of site density were determined via chemical and an electrochemical method. Turnover frequency was evaluated by combining information from RRDE measurements and the measured site density. The data obtained will be used to correlate different catalyst characteristics to their activity, stability and selectivity. The key metrics of the benchmark catalysts will be used as a baseline for the properties of newly synthesised catalysts.

5. REFERENCE

- [1] K. Artyushkova, I. Matanovic, B. Halevi, P. Atanassov, Oxygen Binding to Active Sites of Fe-N-C ORR Electrocatalysts Observed by Ambient-Pressure XPS, *Journal of Physical Chemistry C*. 121 (2017) 2836–2843. doi:10.1021/acs.jpcc.6b11721.